We are IntechOpen, the world's leading publisher of Open Access books
Built by scientists, for scientists

5,600
Open access books available

138,000
International authors and editors

175M
Downloads

Our authors are among the

154
Countries delivered to

TOP 1%
most cited scientists

12.2%
Contributors from top 500 universities

CLARIVATE ANALYTICS
BOOK CITATION INDEX
INDEXED

WEB OF SCIENCE™

Selection of our books indexed in the Book Citation Index
in Web of Science™ Core Collection (BKCI)

Interested in publishing with us?
Contact book.department@intechopen.com

Numbers displayed above are based on latest data collected.
For more information visit www.intechopen.com

Guidance-Based Motion Planning of Autonomous Systems

Bülent Özkan

Abstract

Motion planning is a significant stage in the control of autonomous systems. As an alternative method, guidance approach is proposed for the motion planning of those systems. In guided munitions, guidance laws determine the success of the guidance systems designed to steer systems such as missiles and guided bombs towards predefined targets. The guidance laws designated according to determinative agents such as the firing position of the munition, target type, and operational requirements try to provide the munition with arriving at the target point even under the disturbing effects. In this study, the applicability of the guidance laws to autonomous systems is investigated in a manner similar to the approach for the guided munitions. For this purpose, the motion planning of the selected robotic arm, tracked land vehicle, and quadrotor is tried to be performed in order to move them to predefined target points. Having designed the control systems compatible to the selected guidance laws for the considered systems, the corresponding guidance scheme is constructed. Eventually, after conducting the relevant computer simulations, it is observed that the desired target chase can be made in a successive manner for all cases.

Keywords: motion planning, guidance, guidance law, linear homing, autonomous system

1. Introduction

Motion planning constitutes one of the primary stages in the control of autonomous systems. The autonomous systems can perform their planned tasks under several environmental conditions as per the designated motion planning algorithms in accordance certain performance criteria. The mentioned criteria may include minimum energy or minimum time consumption and shortest path length. For the motion planning purpose, several different algorithms are proposed by relevant researchers. These methods have certain advantages and disadvantages over the others [1–4].

As an alternative approach, guidance schemes can be used in motion planning. Those schemes involve an upper-level guidance algorithm and a lower-level control system. In fact, guidance and control loops can be introduced as officer and soldier, respectively. In other words, as the guidance algorithm behaves as the "master," the control system takes the "slave" role in this scene [5].

The guidance schemes are widely implemented to munitions. Guidance and control systems are designed in a compatible manner with munition dynamics so that the munitions including missiles and guided bombs can carry payloads towards specified target points as planned. The guidance part of the mentioned guidance

and control system constitutes the kinematic relationships established as per the relative position between the munition and intended target point, while the control system is the closed-loop control system constructed based on the dynamic model of the munition under consideration in order to realize the guidance commands generated by the guidance part. In this extent, the guidance approach enrolls as a motion planning scheme for the munition [5].

The type of the command yielded by the guidance system depends on the selected guidance law. Namely, as the output of the proportional navigation guidance law which constitutes the most widely used guidance law in guided munitions is the lateral component of the linear acceleration vector of the munition or change of the lateral angular component of the linear velocity vector in time as per the application, the command of the body pursuit guidance law becomes the components of the angle between the body longitudinal axis of the munition and the lateral axis of the Earth-fixed frame [5, 6].

Guidance laws designated to move the guided munitions towards specified target points make their motion planning in a sense. Regarding this property, there seems no serious obstacle on their implementation on autonomous systems other than guided munition. In this study, the orientation of the sample autonomous mechatronic systems involving a robotic arm, tracked land vehicle, and quadrotor to predefined target points using the linear homing guidance (LHG) law and the relevant computer simulations is carried out. Here, these systems are chosen as very common systems encountered in the physical world. In the considered cases, the LHG law is an angle-based approach, and it takes the flight path angle components of the systems into consideration. Also, the selection of the mentioned mechatronic systems allows evaluating the convenience of the proposed approach in the planar and spatial engagement situations. Moreover, single- and two-stage control systems are utilized in accordance with the LHG law.

Guidance-based motion planning schemes are developed for certain robotic arm configurations [7]. In this scene, the indicated strategy allows the operators to run the moving belt of the robotic arm-belt assembly line within a mounting line in a more continuous and faster manner than the usual methods. Moreover, it may become to suppress or at least minimize the drawbacks of the conventional approaches by regarding the guidance-based motion planning method. Namely, although many conventional methods require the belt assembly to halt at intermediate placing instants, the guidance-based approach makes possible to place the objects under consideration onto the belt while it remains running during operation [8].

Different from wheeled vehicles, tracked land vehicles are directed as per a sliding motion which depends on the rotation of the vehicle about an instantaneous rotation center. In other words, they can be oriented to left or right by rotating about their instantaneous rotation center in the convenient sense. Regarding the motion of these vehicles on soil surfaces especially, the motion planning becomes harder. As a remedy to this inconvenience, the guidance-based path planning approach is proposed in the present study [8].

As the third application, the motion planning of a quadrotor which is intended to carry a payload from a stationary initial point to a prescribed moving land platform at a moderate distance for either military or civil purpose is investigated. Here, the payload can be munition, food, or first aid material. Since the moving platform specified as the target is assumed to be far away from the initial point, it is desired for the quadrotor to catch it within the shortest time duration possible and consume the energy at a minimum level [8, 9].

In the computer simulations in which the planar motion of the robotic arm and tracked land vehicle and the spatial motion of the quadrotor are taken into consideration, it is assumed that the targets are moving along specified trajectories. Here,

regarding the motion characteristics of the autonomous systems dealt with, the robotic arm operates on the horizontal plane, and the vertical displacement of the tracked land vehicle is in a negligible level compared to its longitudinal and lateral motion on the ground plane. Thus, the motion profiles are described on a plane for both the systems. Unlike them, the quadrotor flies in the sky towards all three directions. This fact leads to handle its dynamic behavior in a three-dimensional space. Having completed the computer simulations, it is observed that all three systems can be carried to the intended target points by LHG law [8].

As a motion planning strategy, guidance approach can be applied to service robots which are utilized to accomplish certain motion profiles apart from the industrial systems. In this way, it is intended to perform hazardous, tedious, and time-consuming tasks in a more efficient and accurate manner in daily use. The mentioned category for service robots, actually, involves not only articulated robot manipulators but also moving and flying autonomous structures as well.

2. Description of the systems

2.1 Description of the robotic arm

The schematic views of the robotic arm and mounting line, i.e., trajectory, containing the slot on which the component grasped by the gripper of the arm is placed is given in **Figure 1**.

The system whose schematic view is presented in **Figure 1** consists of a two-degree-of-freedom robotic arm and moving mounting line. Here, the object to be put on the slot on the mounting line by the gripper of the robotic arm is taken in spherical geometry, and thus its orientation is ignored. This way, the degree of freedom of the carried object is reduced to two. In other words, it becomes possible to define the instantaneous planar location of the object by regarding the lateral and vertical position components of a point, i.e., point P, on the object. So, a robotic arm is required with minimum degree of freedom of two in order for the object with two degrees of freedom to be carried upon a specified point on the plane without any control deficiency. The definitions made in **Figure 1** are listed as follows [8]:

x and y: lateral and vertical axes of the Earth-fixed frame symbolized by F_0.

$\vec{u}_1^{(0)}$ and $\vec{u}_2^{(0)}$: unit vectors denoting the x- and y-axis of F_0.
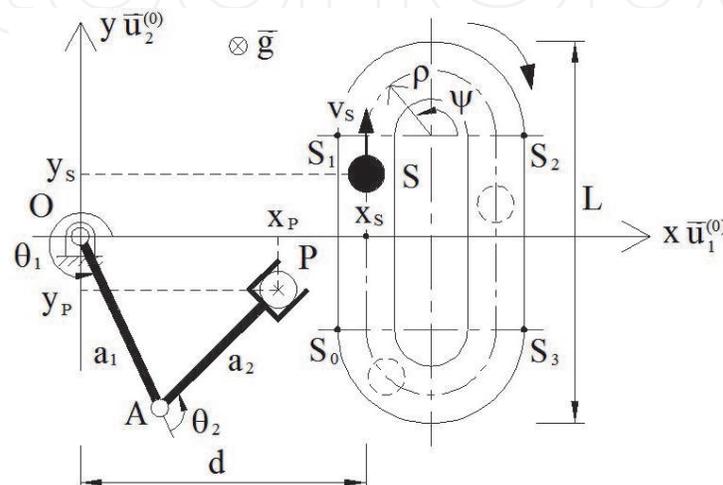
O and A: joints of the robotic arm.

Figure 1.
System consisting of a robotic arm and moving mounting line [8].

a_1 and a_2: lengths of the first and second links of the arm.

θ_1 and θ_2: first and second joint angles of the robotic arm.

P: point defined on the gripper of the robotic arm.

x_P and y_P: lateral and vertical position components of point P.

S: midpoint of the slot on the mounting platform.

S_i: form changing points of the mounting line (i = 1, 2, 3, and 4).

v_S: speed of the slot on the mounting line.

x_S and y_S: lateral and vertical position components of point S.

ρ: turn radius of the mounting line.

ψ: rotation angle on the circular tip parts of the mounting line.

L: total length of the mounting line.

d: perpendicular distance between the connection point of the robotic arm to the ground and the point of the mounting line closest to that connection point.

$\vec{g}$: gravity vector (g = 9.81 m/s^2).

Regarding these definitions, the mathematical model of the robotic arm can be expressed in a compact matrix form as follows [8]:

$$\overline{T} = \hat{M}(\overline{\theta})\ddot{\overline{\theta}} + \hat{H}\left(\dot{\overline{\theta}}, \overline{\theta}\right)\dot{\overline{\theta}} \tag{1}$$

where, as $\overline{\theta} = [\theta_1 \; \theta_2]^T$ and $\overline{T} = [T_1 \; T_2]^T$, $\hat{M}(\overline{\theta})$ and $\hat{H}\left(\dot{\overline{\theta}}, \overline{\theta}\right)$ which denote the inertia matrix and compound friction and Coriolis effect matrix, respectively, are defined as $\hat{M}(\overline{\theta}) = \begin{bmatrix} m_{11} & m_{12} \\ m_{12} & m_{22} \end{bmatrix}$ and $\hat{H}\left(\dot{\overline{\theta}}, \overline{\theta}\right) = \begin{bmatrix} h_{11} & h_{12} \\ h_{21} & h_{22} \end{bmatrix}$ with $m_{11} = m_1 d_1^2 + m_2\left[a_1^2 + d_2^2 + 2a_1 d_2 \cos(\theta_2)\right] + I_{c1} + I_{c2}$, $m_{12} = m_2 d_2[d_2 + a_1 \cos(\theta_2)] + I_{c2}$, $m_{22} = m_2 d_2^2 + I_{c2}$, $h_{11} = b_1 - 2m_2 a_1 d_2 \dot{\theta}_2 \sin(\theta_2)$, $h_{12} = b_2 - m_2 a_1 d_2 \dot{\theta}_2 \sin(\theta_2)$, $h_{21} = m_2 a_1 d_2 \dot{\theta}_1 \sin(\theta_2)$, and $h_{22} = b_2$ [8].

In the shorthand definitions above, m_1, m_2, I_{c1}, and I_{c2} denote the masses of the first and second links of the manipulator and the moments of inertia of these links with respect to their mass centers indicated by C_1 and C_2, respectively. Also, b_1 and b_2 represent the viscous friction coefficients at the first and second joints as well as the definitions of $d_1 = |OC_1|$ and $d_2 = |AC_2|$ [8].

2.2 Description of the tracked land vehicle

As the second system examined, the schematic description of the tracked land vehicle is shown in **Figure 2**. The explanations of the quantities labeled in **Figure 2** are given as follows [8]:

O, G, and C: origin of F_0, mass canter of the tracked vehicle, and instantaneous rotation center of the vehicle.

$\vec{u}_i^{(0)}$: unit vectors of F_0.

$\vec{u}_i^{(b)}$: unit vectors of the tracked land vehicle frame, i.e., F_b.

x and y: position components of point G on F_0.

ψ: orientation angle of the vehicle on the vertical plane.

$\vec{r}_{G/O}$: relative position of point G with respect to point O.

$\vec{r}_{G/C}$: relative position of point G with respect to point C.

x_C and y_C: position components point C in F_b.

a, b, c, d, and v: dimensional parameters of the vehicle.

m: mass of the tracked land vehicle.

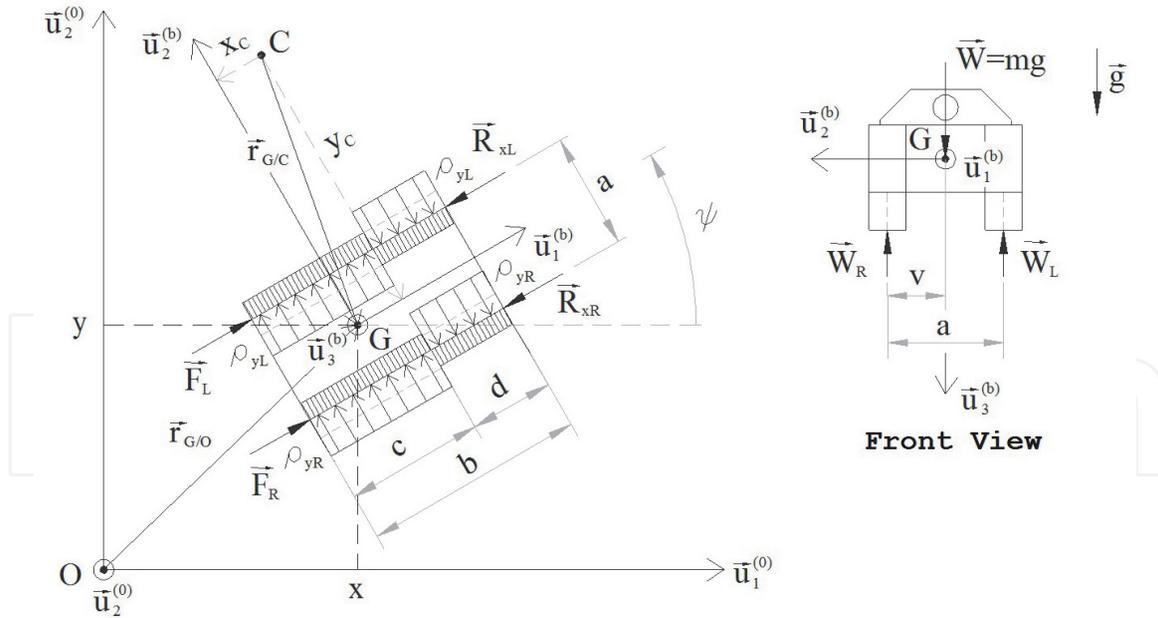$\vec{W}$: weight vector of the tracked land vehicle.

Figure 2.
Notable kinematic parameters of the tracked land vehicle and forces acting on the vehicle [8].

$\vec{W}_L$ and $\vec{W}_R$: weighting forces on the left and right tracks.

$\vec{R}_{XL}$ and $\vec{R}_{XR}$: longitudinal friction components acting on the left and right tracks.

$\vec{F}_L$ and $\vec{F}_R$: actuation forces acting on the left and right tracks.

ρ_{xL} and ρ_{xR}: lateral friction force density acting on the left and right tracks.

For the tracked land vehicle, as u_x, u_y, and u_z denote the inputs and b_x, b_y, and b_ψ indicate the gravity and frictional force components, governing differential equations can be written in the following manner [8]:

$$\ddot{x} = u_x - b_x \tag{2}$$

$$\ddot{y} = u_y - b_y \tag{3}$$

$$\ddot{\psi} = u_\psi + b_\psi \tag{4}$$

where $u_x = u_F \cos(\psi)$, $u_y = u_F \sin(\psi)$, $u_F = (T_L + T_R)/(m r_S)$, $u_\psi = a(T_R - T_L)/(2 I_z r_S)$, $b_x = \sigma_{\dot{x}} \mu_x g \cos(\psi)$, $b_y = \sigma_{\dot{x}} \mu_x g \sin(\psi)$, and $b_\psi = \frac{\sigma_{\dot{\psi}} m g}{b I_z} \left[b \sigma_{\dot{x}} \left(v - \frac{a}{2} \right) \left(\frac{\mu_x}{\mu_y} \right) + x_C (c - d) - \frac{(c^2 + d^2)}{2} \right]$.

Regarding these definitions, T_L and T_R stand for the actuation torques exerted by the power transmission gears on the left and right tracks; r_S and I_z represent the radius of its actuation gear and moment of inertia of the vehicle about the rotation axis indicated by the unit vector $\vec{u}_3^{(b)}$; and eventually μ_x and μ_y stand for the static friction coefficients between the tracks of the vehicle and surface on the lateral planes. Here, the symbols $\sigma_{\dot{x}}$ and $\sigma_{\dot{\psi}}$ are introduced as $\sigma_{\dot{x}} = \text{sgn}[\dot{x}\cos(\psi) + \dot{y}\sin(\psi)]$ and $\sigma_{\dot{\psi}} = \text{sgn}(\dot{\psi})$ where sgn($\cdot$) shows the signum function [8].

2.3 Description of the quadrotor

The schematic view of the quadrotor, the third system under consideration, and engagement geometry between the quadrotor and moving land platform are presented in **Figures 3** and **4**, respectively [8].
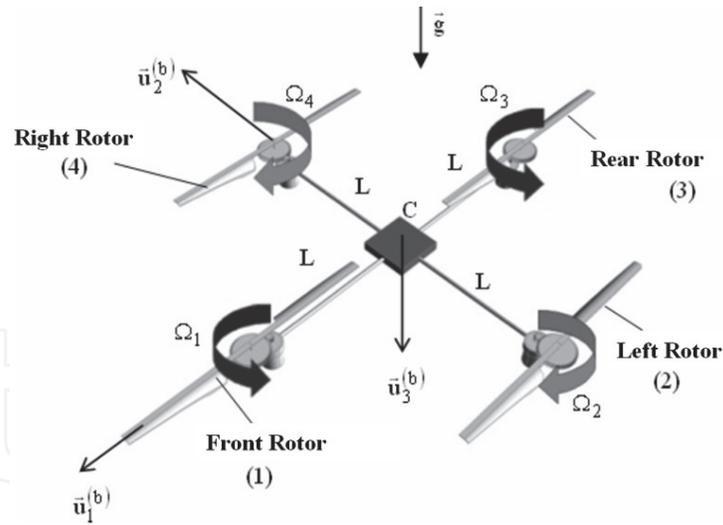
Figure 3.
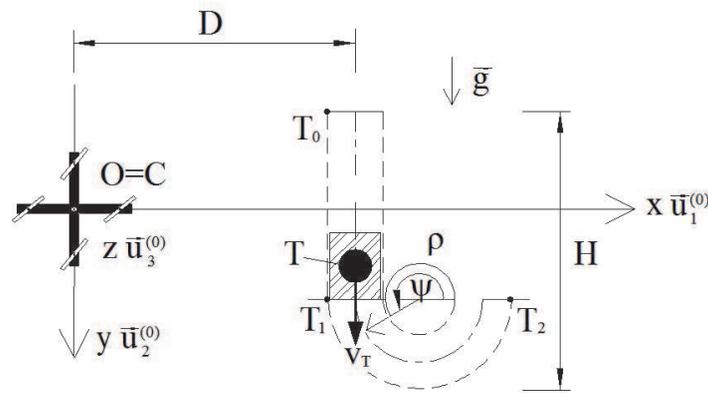*Schematic view of the quadrotor [8].*

Figure 4.
Engagement geometry for the quadrotor [8].

As indicated in **Figure 3**, the front and rear rotors expressed as numbers 1 and 3, respectively, have rotations in positive sense around the axis represented by unit vector $\vec{u}_3^{(b)}$ of the body-fixed frame of the quadrotor, i.e., F_b, whose origin is attached at point C and whose axes are shown by unit vectors $\vec{u}_i^{(b)}$ (i = 1, 2, and 3), while the left and right rotors, i.e., numbers 2 and 4 rotors, rotate in negative sense [8].

In **Figure 3**, L and Ω_j (j = 1, 2, 3, and 4) stand for the distance between the center of rotation of each motor and point C and angular speed of the electromechanical actuator, i.e., electrical servomotor, used to move the propeller j, respectively. In addition to those parameters, the symbols in **Figure 3** can be listed as follows [8]:

T: target point on the moving platform for the quadrotor.
T_i: points at which the shape of the trajectory of the moving platform changes (i = 0, 1, and 2).
v_T: linear speed of point T on the moving platform.
ρ: radius of curvature of the trajectory of the moving platform.
ψ: rotation angle of the rounded tip portions of the trajectory of the moving platform.
H: total length of the trajectory of the moving platform.
D: perpendicular distance between the origin of F_0, i.e., point O, and the midline of the section of the trajectory of the moving platform closest to this point.

Considering the related kinematic and dynamic parameters of the quadrotor system, the dynamic model of the quadrotor can be set as follows using the relevant kinematic and dynamic parameters with angular position parameters of ϕ, θ, and ψ and translational position parameters of x, y, and z [8]:

$$\ddot{\phi} = -c_\phi \dot{\phi} + J_{\psi\theta}\dot{\psi}\dot{\theta} + J_\theta\Omega_e\dot{\theta} + u_\phi \tag{5}$$

$$\ddot{\theta} = -c_\theta\dot{\theta} + J_{\psi\phi}\dot{\psi}\dot{\phi} - J_\phi\Omega_e\dot{\phi} + u_\theta \tag{6}$$

$$\ddot{\psi} = -c_\psi\dot{\psi} + J_{\theta\phi}\dot{\theta}\dot{\phi} + u_\psi \tag{7}$$

$$\ddot{x} = -c_x\dot{x} + u_x \tag{8}$$

$$\ddot{y} = -c_y\dot{y} + u_y \tag{9}$$

$$\ddot{z} = -c_z\dot{z} - g + u_z \tag{10}$$

where $c_\phi = LK_\phi/J_x$, $J_{\psi\theta} = \left(J_y - J_z\right)/J_x$, $J_\theta = J_v/J_x$, $\Omega_e = \Omega_1 - \Omega_2 + \Omega_3 - \Omega_4$, $u_\phi = Lb\left(\Omega_2^2 - \Omega_4^2\right)/J_x$, $c_\theta = LK_\theta/J_y$, $J_{\psi\phi} = (J_z - J_x)/J_y$, $J_\phi = J_v/J_y$, $u_\theta = Lb\left(\Omega_1^2 - \Omega_3^2\right)/J_y$, $c_\psi = K_\psi/J_z$, $J_{\theta\phi} = \left(J_x - J_y\right)/J_z$, $u_\psi = d\left(-\Omega_1^2 + \Omega_2^2 - \Omega_3^2 + \Omega_4^2\right)/J_z$, $c_x = K_x/m$, $u_x = b\left(\Omega_1^2 + \Omega_2^2 + \Omega_3^2 + \Omega_4^2\right)[c(\psi)s(\theta)c(\phi) + s(\psi)s(\phi)]/m$, $c_y = K_y/m$, $u_y = b\left(\Omega_1^2 + \Omega_2^2 + \Omega_3^2 + \Omega_4^2\right)[s(\psi)s(\theta)c(\phi) - c(\psi)s(\phi)]/m$, $c_z = K_z/m$, and $u_z = b\left(\Omega_1^2 + \Omega_2^2 + \Omega_3^2 + \Omega_4^2\right)c(\theta)c(\phi)/m$.

In the definitions above, J_x, J_y, and J_z show the moment of inertia components of the quadrotor around the axes defined by unit vectors $\vec{u}_1^{(b)}$, $\vec{u}_2^{(b)}$, and $\vec{u}_3^{(b)}$, respectively. J_v represents the moment of inertia of each rotor about its axis of rotation, d indicates the drag factor, and K_ϕ, K_θ, K_ψ, K_x, K_y, and K_z stand for the aerodynamic moment and force components acting on the system in the roll, pitch, and yaw planes and along the longitudinal, lateral, and vertical planes, respectively. Furthermore, b indicates thrust factor of the motors [8].

3. Control systems

Since the guidance commands generated by the LHG law which is considered to make the motion planning of the autonomous systems so as to bring them to the specified point on the target trajectories are in terms of the linear velocity components of the mass centers of those systems, the main control variables of the systems are selected to be velocity components [8]. Also, for the sake of maintaining the stability of the systems, the gain matrices of the relevant control systems are continuously updated throughout the planned motion using the state information of target acquired by certain means like a camera.

3.1 Robotic arm control system

Because the guidance signals produced by the LHG law are in terms of the angle between the velocity vector of point P and lateral axis, the control variable of the robotic arm control system is chosen to be the joint speeds, i.e., $\dot{\theta}_1$ and $\dot{\theta}_2$ [6]. Since the main objective is the speed control of point P, the control system based on the joint speeds corresponds to an indirect control scheme. Regarding the difficulty in the measurement of the instantaneous speed values of point P along with the fact that joint angles and their rates can easily be acquired by means of the sensors put

on the joints, the use of such an indirect control algorithm seems to be proper. In this sense, the linear position and velocity components of point P can be calculated using the measured joint positions and speeds via the loop closure equations, and consequently the trajectory of point P on the horizontal plane can be determined as a function of time [8].

Here, as $\dot{\theta}_{1d}$ and $\dot{\theta}_{2d}$ indicate the reference joint speeds and $\dot{\overline{\theta}}_d = \begin{bmatrix} \dot{\theta}_{1d} & \dot{\theta}_{2d} \end{bmatrix}^T$ stands for the column matrix corresponds to these quantities, the error between the desired, i.e., reference, and actual joint speeds, i.e., $\overline{e}$, can be set as follows [8]:

$$\overline{e} = \dot{\overline{\theta}}_d - \dot{\overline{\theta}} \tag{11}$$

The relevant control rule can be written according to the computed torque method with the addition of the integral action to nullify the steady-state errors by regarding the error definition in Eq. (11) as follows [10]:

$$\overline{T} = \hat{M}\ddot{\overline{\theta}}_d + \hat{H}\dot{\overline{\theta}} + \hat{K}_p\overline{e} + \hat{K}_i \int \overline{e}\,dt \tag{12}$$

Here, as "T" represents the matrix transpose, $\overline{T} = \begin{bmatrix} T_1 & T_2 \end{bmatrix}^T$ demonstrates the torque column matrix for joint torques T_1 and T_2. Also, $\hat{M} = \hat{M}(\overline{\theta})$ and $\hat{H} = \hat{H}\left(\overline{\theta}, \dot{\overline{\theta}}\right)$ denote the inertia and centrifugal effect matrices, while $\hat{K}_p$ and $\hat{K}_i$ correspond to the proportional and integral gain matrices, respectively. As implied, the resulting control system becomes in PI (proportional plus integral) form [8].

The differential equation corresponding to the error dynamics of the control system for the robotic arm are obtained using Eqs. (11) and (12) in the following fashion:

$$\ddot{\overline{e}} + \hat{M}^{-1}\left(\dot{\hat{M}} + \hat{K}_p\right)\dot{\overline{e}} + \hat{M}^{-1}\hat{K}_i\overline{e} = \overline{0} \tag{13}$$

As ω_{ci} and ζ_{ci} denote the desired bandwidth and damping ratio of link i (i = 1 and 2), the error dynamics can be written for a second-order ideal system with two degrees of freedom as follows [10]:

$$\ddot{\overline{e}} + \hat{D}\dot{\overline{e}} + \hat{W}\overline{e} = \overline{0} \tag{14}$$

where $\hat{D} = \begin{bmatrix} 2\zeta_{c1}\omega_{c1} & 0 \\ 0 & 2\zeta_{c2}\omega_{c2} \end{bmatrix}$ and $\hat{W} = \begin{bmatrix} \omega_{c1}^2 & 0 \\ 0 & \omega_{c2}^2 \end{bmatrix}$.

Consequently, $\hat{K}_p$ and $\hat{K}_i$ are determined by equating Eq. (13) to Eq. (14) as follows [8]:

$$\hat{K}_p = \hat{M}\hat{D} - \dot{\hat{M}} \tag{15}$$

$$\hat{K}_i = \hat{M}\hat{W} \tag{16}$$

3.2 Tracked land vehicle control system

During the control of the tracked land vehicle for the angular variables, the angular position requirement for ψ should also be satisfied. For this purpose, a two-stage cascaded control scheme is constructed for the tracked land vehicle. In this algorithm, the outer loop is responsible of making linear velocity control in accordance with the guidance commands, while the inner loop makes the angular

position control such that the orientation angle requirement arising during the linear velocity control is realized [8].

Here, the expressions which will be considered for the design of the linear velocity control system which is termed as "the primary control system" can be arranged in the forthcoming state space form from Eqs. (2) and (3) as $\overline{x}_p = [\dot{x} \quad \dot{y}]^T$, $\overline{u}_p$, and $\overline{b}_p$ stand for the column matrices for the state variables, system inputs, and gravity effect, respectively [8]:

$$\dot{\overline{x}}_p = -\overline{b}_p + \overline{u}_p \tag{17}$$

The control rule of the primary control system can be established using the computed torque control method according to the PI control action like the robotic arm control system so as to nullify the steady-state errors [8]:

$$\overline{u}_p = \dot{\overline{x}}_{pd} + \overline{b}_p + \hat{K}_{pp}\overline{e}_p + \hat{K}_{pi}\int \overline{e}_p \, dt \tag{18}$$

In the above equation, $\overline{x}_{pd}$, $\hat{K}_{pp}$, $\hat{K}_{pi}$, and $\overline{e}_p$ denote the column matrix for the desired inputs, gain matrix for the proportional control action, gain matrix for the integral control action, and column matrix for the error, respectively, for the primary control system. Here, $\overline{e}_p = \overline{x}_{pd} - \overline{x}_p$ is introduced.

Substituting Eq. (18) into Eq. (17) yields the next equation for the error dynamics of the primary control system [8]:

$$\ddot{\overline{e}}_p + \hat{K}_{pp}\dot{\overline{e}}_p + \hat{K}_{pi}\overline{e}_p = \overline{0} \tag{19}$$

As ω_{pi} and ζ_{pi} denote the desired bandwidth and damping ratio of link i (i = 1 and 2) for the primary control system, the error dynamics can be written for a second-order ideal system with two degrees of freedom as follows [8]:

$$\ddot{\overline{e}}_p + \hat{D}_p\dot{\overline{e}}_p + \hat{W}_p\overline{e}_p = \overline{0} \tag{20}$$

where $\hat{D}_p = \begin{bmatrix} 2\zeta_{p1}\omega_{p1} & 0 \\ 0 & 2\zeta_{p2}\omega_{p2} \end{bmatrix}$ and $\hat{W}_p = \begin{bmatrix} \omega_{p1}^2 & 0 \\ 0 & \omega_{p2}^2 \end{bmatrix}$.

Equating Eq. (19) to Eq. (20), the gain matrices are found for the primary control system as follows [8]:

$$\hat{K}_{pp} = \hat{D}_p \tag{21}$$

$$\hat{K}_{pi} = \hat{W}_p \tag{22}$$

The control rule for the angular control system called "the secondary control system" can be set using the computed torque method according to the PD (proportional plus derivative) control action in the following fashion [8]:

$$u_\psi = \ddot{\psi}_d - b_\psi + K_{sp}e_s + K_{sd}\dot{e}_s \tag{23}$$

In the above expression, b_ψ, ψ_d, K_{sp}, K_{sd}, and e_s represent the inertia gain for the vehicle, desired input variable for the secondary control system, gain of the proportional control action, gain of the derivative control action, and error, respectively. Also, $e_s = \psi_d - \psi$ is introduced.

Plugging Eq. (23) into Eq. (4), the error dynamics of the secondary control system is determined as follows [8]:

$$\ddot{e}_s + K_{sd}\dot{e}_s + K_{sp}e_s = 0 \tag{24}$$

As ω_s and ζ_s indicate the desired bandwidth and damping ratio for variable ψ for the secondary control system, the error dynamics can be written for a second-order ideal system with single degree of freedom as given below:

$$\ddot{e}_s + 2\zeta_s\omega_s\dot{e}_s + \omega_s^2 e_s = 0 \tag{25}$$

Matching Eqs. (24) and (25) results in the forthcoming gains for the secondary control system [8]:

$$K_{sp} = \omega_s^2 \tag{26}$$

$$K_{sd} = 2\zeta_s\omega_s \tag{27}$$

3.3 Quadrotor control system

The same two-stage control system is designed for the quadrotor as that for the tracked land vehicle. For the primary control system, these expressions can be rearranged in the state space form by assigning the columns of the state variables and inputs of the system to be $\overline{x}_p = \begin{bmatrix} \dot{x} & \dot{y} & \dot{z} \end{bmatrix}^T$ and $\overline{u}_p = \begin{bmatrix} u_x & u_y & u_z \end{bmatrix}^T$, respectively, as letter "T" indicates the transpose operation as follows [8]:

$$\dot{\overline{x}}_p = -\hat{C}_p\overline{x}_p + \overline{u}_p \tag{28}$$

where $\hat{C}_p = \begin{bmatrix} c_x & 0 & 0 \\ 0 & c_y & 0 \\ 0 & 0 & c_z \end{bmatrix}$.

The control law of the primary control system including an integral action can be designed as per the computed torque method with PI action in the following manner [8]:

$$\overline{u}_p = \dot{\overline{x}}_{pd} + \hat{C}_p\overline{x}_p + \hat{K}_{pp}\overline{e}_p + \hat{K}_{pi}\int \overline{e}_p\,dt \tag{29}$$

In the expression above, $\overline{x}_{pd}$, $\hat{K}_{pp}$, $\hat{K}_{pi}$, and $\overline{e}_p$ stand for the desired input column, proportional gain matrix, integral gain matrix, and error column for the primary control system, respectively, and the definition $\overline{e}_p = \overline{x}_{pd} - \overline{x}_p$ is given.

Substituting Eq. (29) into Eq. (28), the error dynamics of the primary control system is obtained as follows [8]:

$$\ddot{\overline{e}}_p + \hat{K}_{pp}\dot{\overline{e}}_p + \hat{K}_{pi}\overline{e}_p = \overline{0} \tag{30}$$

As ω_{pi} and ζ_{pi} represent the desired bandwidth and damping ratio of the ith state variable (i = 1, 2, and 3) of the primary control system, respectively, the error dynamics of a second-order ideal system with three degrees of freedom can be described using the forthcoming expression [8]:

$$\ddot{\overline{e}}_p + \hat{D}_p\dot{\overline{e}}_p + \hat{W}_p\overline{e}_p = \overline{0} \tag{31}$$

where $\hat{D}_p = \begin{bmatrix} 2\zeta_{p1}\omega_{p1} & 0 & 0 \\ 0 & 2\zeta_{p2}\omega_{p2} & 0 \\ 0 & 0 & 2\zeta_{p3}\omega_{p3} \end{bmatrix}$ and $\hat{W}_p = \begin{bmatrix} \omega_{p1}^2 & 0 & 0 \\ 0 & \omega_{p2}^2 & 0 \\ 0 & 0 & \omega_{p3}^2 \end{bmatrix}$.

Matching Eqs. (30) and (31), the gain matrices appear for the primary control system as follows:

$$\hat{K}_{pp} = \hat{D}_p \tag{32}$$

$$\hat{K}_{pi} = \hat{W}_p \tag{33}$$

As the corresponding columns of the state variables and inputs of the system are shown to be $\bar{x}_s = \begin{bmatrix} \phi & \theta & \psi \end{bmatrix}^T$ and $\bar{u}_s = \begin{bmatrix} u_\phi & u_\theta & u_\psi \end{bmatrix}^T$, the matrix equality below is reached via Eqs. (5)–(7) for the orientation, or attitude, control system as the secondary control system [8]:

$$\ddot{\bar{x}}_s = \bar{b}_s + \bar{u}_s \tag{34}$$

where $\bar{b}_s = \begin{bmatrix} -c_\phi\dot{\phi} + (J_{\psi\theta}\dot{\psi} + J_\theta\Omega_e)\dot{\theta} & -c_\theta\dot{\theta} + (J_{\psi\phi}\dot{\psi} - J_\phi\Omega_e)\dot{\phi} & -c_\psi\dot{\psi} + J_{\theta\phi}\dot{\theta}\dot{\phi} \end{bmatrix}^T$.

In a similar manner, the control law can be written according to the computed torque method with PD action for the secondary control system as follows [8]:

$$\bar{u}_s = \ddot{\bar{x}}_{sd} - \bar{b}_s + \hat{K}_{sp}\bar{e}_s + \hat{K}_{sd}\dot{\bar{e}}_s \tag{35}$$

Here, $\bar{x}_{sd}$, $\hat{K}_{sp}$, $\hat{K}_{sd}$, and $\bar{e}_s$ indicate the desired input column, proportional gain matrix, derivative gain matrix, and error column for the secondary control system, respectively. Also, the definition $\bar{e}_s = \bar{x}_{sd} - \bar{x}_s$ is made for the error term.

In the proposed entire control scheme, the desired values of ϕ and θ are calculated using u_x, u_y, and u_z inputs along with the parameter u_F by regarding the definitions within Eqs. (5)–(10). In other words, the reference inputs, or commands, to ϕ and θ are generated by the outer loop. On the other hand, the remaining angular position variable ψ is adjusted to be a constant value. That means its reference value is set as a fixed quantity. In this sense, the desired value of ψ is then specified to be zero as the decision on keeping the quadrotor with no angular motion in the yaw plane [11, 12].

Inserting Eq. (35) into Eq. (34), the error dynamics of the secondary control system is obtained as

$$\ddot{\bar{e}}_s + \hat{K}_{sd}\dot{\bar{e}}_s + \hat{K}_{sp}\bar{e}_s = \bar{0} \tag{36}$$

As ω_{si} and ζ_{si} denote the desired bandwidth and damping ratio of the ith state variable (i = 1, 2, and 3) of the secondary control system, the error dynamics of a second-order ideal system with three degrees of freedom can be described using the following equation [8]:

$$\ddot{\bar{e}}_s + \hat{D}_s\dot{\bar{e}}_s + \hat{W}_s\bar{e}_s = \bar{0} \tag{37}$$

where $\hat{D}_s = \begin{bmatrix} 2\zeta_{s1}\omega_{s1} & 0 & 0 \\ 0 & 2\zeta_{s2}\omega_{s2} & 0 \\ 0 & 0 & 2\zeta_{s3}\omega_{s3} \end{bmatrix}$ and $\hat{W}_s = \begin{bmatrix} \omega_{s1}^2 & 0 & 0 \\ 0 & \omega_{s2}^2 & 0 \\ 0 & 0 & \omega_{s3}^2 \end{bmatrix}$.

Equating Eqs. (47) and (48) to each other yields the gain matrices of the secondary control system as shown below [8]:

$$\hat{K}_{sp} = \hat{W}_s \tag{38}$$

$$\hat{K}_{sd} = \hat{D}_s \tag{39}$$

4. Engagement geometry

Since the motion of the moving land platform for the quadrotor, i.e., trajectory of the target point, is dealt with in the three-dimensional space, the lateral projection of the engagement geometry drawn for the quadrotor can be used for the engagements of the robotic arm and tracked land vehicle with their targets as well.

The engagement geometry between the quadrotor and the moving land platform is described in the horizontal and vertical planes separately. Thus, the vertical engagement between point C, the mass center of the quadrotor, and point T on the moving platform can be depicted as seen in **Figure 5**. The lateral engagement geometry between points C and T can be similarly constructed using the same expressions [8].

In **Figure 5**, v_C, γ_q, $r_{T/C}$, γ_t, and λ_p show the resultant speed of point C, orientation angle of v_C from the horizontal plane, relative position of point T with respect to point C, orientation angle of v_T from the horizontal axis, and orientation angle of $r_{T/C}$ from the horizontal axis. Here, the next equations are held for v_C, γ_t, and λ_p [8]:

$$v_C = \sqrt{\dot{x}_C^2 + \dot{y}_C^2 + \dot{z}_C^2} \tag{40}$$

$$\gamma_t = \begin{cases} -\pi/2, t_0 < t \leq t_1 \\ (\pi/2) - \psi, t_1 < t \leq t_2 \quad \text{(rad)} \\ \pi/2, t > t_2 \end{cases} \tag{41}$$

$$\lambda_p = a \tan\left[(y_T - y_C)/(x_T - x_C)\right] \tag{42}$$

Similarly, the orientation angle of $r_{T/C}$ from the horizontal plane, i.e., λ_y, can be obtained as follows [8]:

$$\lambda_y = a \tan\left[(z_T - z_C)/(x_T - x_C)\right] \tag{43}$$

The final offset between points C and T at the end of the engagement, i.e., d_{miss}, is calculated using the next formula as t_F indicates the termination time [8]:
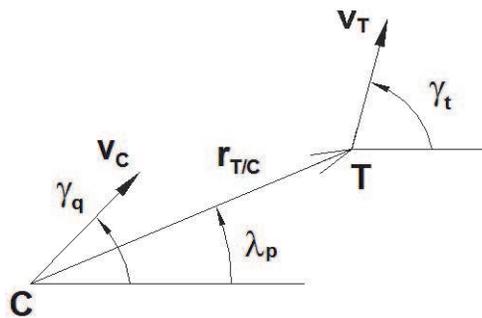

Figure 5.
Vertical engagement geometry between the mass center of the quadrotor and point defined on the moving platform [8].

$$d_{miss} = \sqrt{\Delta x^2(t_F) + \Delta y^2(t_F) + \Delta z^2(t_F)} \qquad (44)$$

Here, as x_C, y_C, and z_C stand for the position components of point C and x_T, y_T, and z_T stand for the position components of point T on F_0, $\Delta x(t_F) = x_C(t_F) - x_T(t_F)$, $\Delta y(t_F) = y_C(t_F) - y_T(t_F)$, and $\Delta z(t_F) = z_C(t_F) - z_T(t_F)$.

5. Guidance law

In order for the considered point on the relevant system (point P for the robotic arm, point C for the tracked land vehicle, and point C for the quadrotor) to catch the desired point on the moving platform (point S for the robotic arm and point T for the tracked land vehicle and quadrotor), the guidance commands can be derived according to the LHG law for which the mechatronic system-target engagement geometry is depicted in **Figure 6** [13].

In **Figure 6**, M, T, and P stand for the mechatronic system, the target, and the predicted intercept point, respectively. Also, $\vec{v}_{Mactual}$ shows the velocity vector of the mechatronic system at the beginning of the guidance. The velocity vector of the mechatronic system in order to be on the collision triangle is then indicated by $\vec{v}_{Mideal}$. Once $\vec{v}_{Mactual}$ is turned into $\vec{v}_{Mideal}$, it means that the mechatronic system is on the collision triangle so as to collide the intended target at point P. In applying this method, unless the target has a velocity vector constant in both magnitude and direction, $\vec{v}_{Mideal}$ should be updated continuously in order to guarantee the intercept [13].

Regarding the LHG geometry expressed above verbally, the relevant guidance commands can be derived in terms of the orientation angles of v_C from the lateral and vertical axes (η_q^c and γ_q^c) as follows [6, 8]:

$$\eta_q^c = a \tan \left[(v_{Ty}\, \Delta t - \Delta y)/(v_{Tx}\, \Delta t - \Delta x) \right] \qquad (45)$$
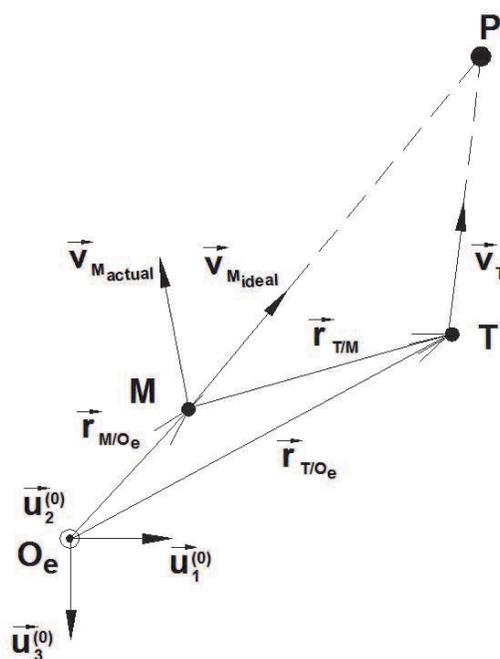

Figure 6.
Linear homing guidance law geometry [13].

$$\gamma_q^c = a \tan \left[\frac{\Delta z - v_{Tz} \, \Delta t}{(v_{Tx} \, \Delta t - \Delta x) \cos\left(\eta_q^c\right) + (v_{Ty} \, \Delta t - \Delta y) \sin\left(\eta_q^c\right)} \right] \qquad (46)$$

where $\Delta x = x_C - x_T$, $\Delta y = y_C - y_T$, and $\Delta z = z_C - z_T$.

In Eqs. (45) and (46), the components of the linear velocity vector of point T whose amplitude is v_T, i.e., v_{Tx}, v_{Ty}, and v_{Tz}, are defined in the following equations [6, 8]:

$$v_{Tx} = v_T \cos(\gamma_t) \qquad (47)$$

$$v_{Ty} = v_T \sin(\gamma_t) \qquad (48)$$

$$v_{Tz} = 0 \qquad (49)$$

Furthermore, the remaining time till the end of the engagement, i.e., Δt, is formulated below:

$$\Delta t = \left[\sqrt{\sigma^2 + (v_C^2 - v_T^2) \, \Delta r^2} - \sigma \right] / (v_C^2 - v_T^2) \qquad (50)$$

In the above equation, $\sigma = v_{Tx} \, \Delta x + v_{Ty} \, \Delta y + v_{Tz} \, \Delta z$ and $\Delta r^2 = \Delta x^2 + \Delta y^2 + \Delta z^2$.

In this work, it is assumed that the speed and orientation parameters of the moving target are obtained by processing the data acquired by the camera on the system under control. Since the control inputs of the designed control system are linear velocity components, the guidance commands given in Eqs. (45) and (46) should be expressed in terms of the linear velocity parameters for realization. This transformation can be done by writing the velocity vector of point C with amplitude v_C in terms of its components on F_0 as follows [6, 8]:

$$\overline{x}_{pd} = v_C \begin{bmatrix} \cos\left(\eta_q^c\right) \cos\left(\gamma_q^c\right) \\ \sin\left(\eta_q^c\right) \cos\left(\gamma_q^c\right) \\ -\sin\left(\gamma_q^c\right) \end{bmatrix} \qquad (51)$$

Parameter	Numerical value
a_1 and a_2	1.25 m
d_1 and d_2	0.625 m
m_1 and m_2	10 kg
I_{c1} and I_{c2}	1.302 kg·m^2
b_1 and b_2	0.001 N·m·s/rad
ω_{c1} and ω_{c2}	10 Hz
ζ_{c1} and ζ_{c2}	0.707
L	2 m
ρ	0.5 m
d	1.5 m

Table 1.
Numerical values used in the simulations for the robotic arm [8].

6. Computer simulations

The system trajectories acquired from the computer simulations performed in accordance with the numerical values given in **Tables 1–3** for the robotic arm, tracked land vehicle, and quadrotor are submitted in **Figures 7–10** along with the corresponding target motions. Having constructed the engagement geometry between the mechatronic system under consideration and target, the LHG law is applied for these situations. In the simulations, disturbance effects due to the nonlinear friction characteristic and noise on the sensors on the joints are assumed

Parameter	Numerical value
a	2.5 m
b	4 m
v	1.25 m
m	25,000 kg
I_z	60,000 kg·m^2
r_s	0.3 m
μ_x and μ_y	0.4
ω_{p1} and ω_{p2}	10 Hz
f_s	30 Hz
ζ_{p1}, ζ_{p2}, and ζ_s	0.707

Table 2.
Numerical values used in the simulations for the tracked land vehicle [8].

Parameter	Numerical value
L	0.25 m
b	5×10^{-5} N·s^2
d	1×10^{-6} N·m·s^2
m	2 kg
I_x and I_y	0.2 kg·m^2
I_z	0.3 kg·m^2
J_v	1×10^{-3} kg·m^2
K_x, K_y, and K_z	0.01 N·s/m
K_ϕ, K_θ, and K_ψ	0.012 N·s/m
ω_{pi}	5 Hz
ω_{si}	15 Hz
ζ_{pi} and ζ_{si}	0.707
H	50 m
ρ	15 m
D	50 m
Solver step	1 ms

Table 3.
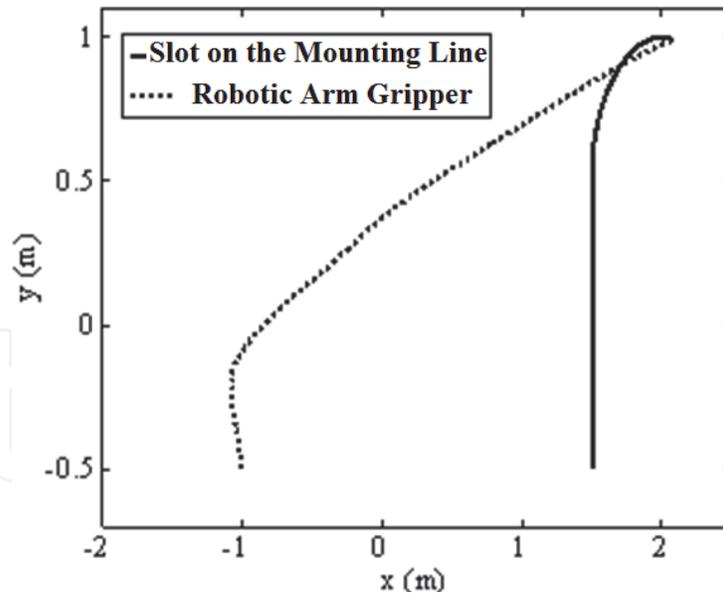*Numerical values used in the simulations for the quadrotor [8].*

Figure 7.
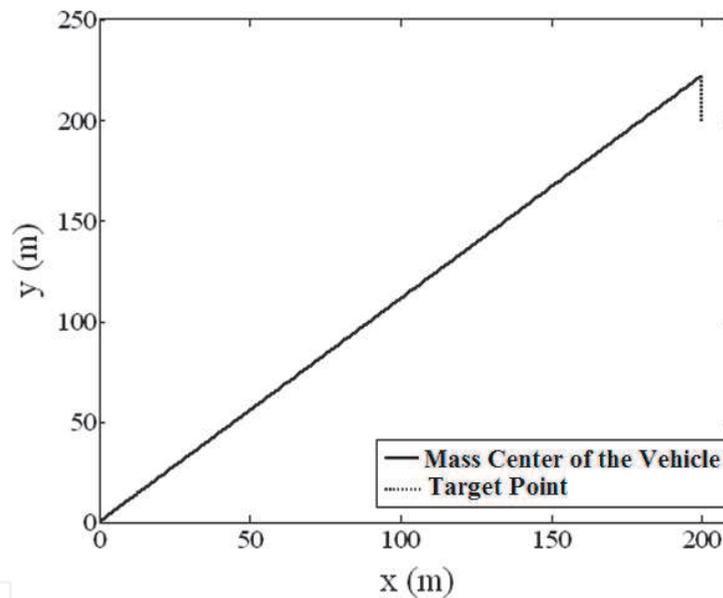*Engagement geometry of the robotic arm with the mounting line.*

Figure 8.
Engagement geometry of the tracked land vehicle with the constant speed target point.

to randomly change within the intervals of ±10 N·m and $\pm1 \times 10^{-3}$ rad for the robotic arm. Also, it is regarded that the angular and linear dynamics of the quadrotor are subjected to random disturbing moment and force with maximum amplitudes of 50 N·m and 100 N, respectively. The simulations of the tracked land vehicle are made on nominal operating conditions [8].

7. Conclusion

As a result of the performed computer simulations, it is shown that the considered autonomous mechatronic systems, i.e., the robotic arm, tracked land vehicle, and quadrotor, can catch the specified target points by regarding the LHG law. Although only one engagement case is presented for each of the systems above, the same result is attained for different situations, too. In this scene, one of the most
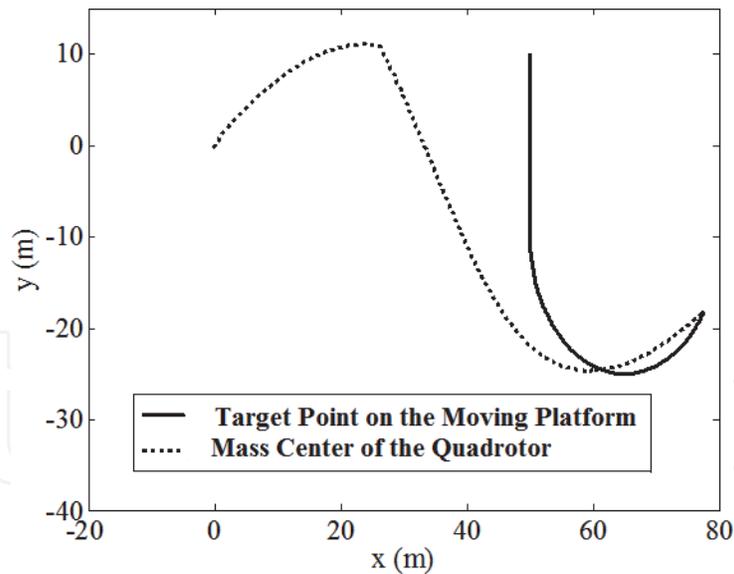
Figure 9.
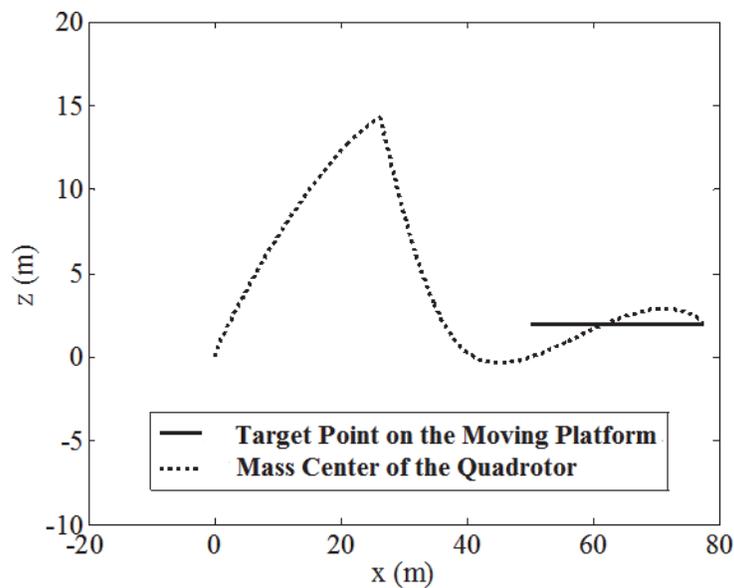*Horizontal engagement geometry of the quadrotor with the platform.*

Figure 10.
Vertical engagement geometry of the quadrotor with the platform.

important considerations is the capacity of the actuators of the autonomous systems. Namely, if the maximum force or torque, hence maximum current, level of the actuators (electric motors) does not satisfy the requirements arising due to the planned motion profile, then the relevant system cannot track the target as planned. In general, it can be concluded that the motion planning of mechatronic systems including the service robots can be made against predefined target points by choosing a convenient guidance law.

Author details

Bülent Özkan
The Scientific and Technological Research Council of Turkey, Defense Industries
Research and Development Institute (TÜBİTAK SAGE), Turkey

*Address all correspondence to: bozkan37@gmail.com

IntechOpen

References

[1] Debnath SSK, Omar R, Latip NBA. A review on energy efficient path planning algorithms for unmanned air vehicles. Computational Science and Technology, Lecture Notes in Electrical Engineering. Singapore: Springer Nature Singapore Pte Ltd.; 2019;**481**:523-532

[2] Mahmoud Zadeh S, Powers DMW, Bairam Zadeh R. State-of-the-art in UVs' autonomous motion planning. Autonomy and Unmanned Vehicles, Cognitive Science and Technology. Singapore: Springer Nature Singapore Pte Ltd.; 2019. pp. 31-40

[3] Du X, Li X, Li D, Dai B. Path planning for autonomous vehicles in complicated environments. In: 2016 IEEE International Conference on Vehicular Electronics and Safety (ICVES); 2016. pp. 54-60

[4] Minh VT, Pumwa J. Feasible path planning for autonomous vehicles. Mathematical Problems in Engineering. 2014;**2014**:1-12

[5] Zarchan P. Tactical and Strategic Missile Guidance. 2nd ed. USA: Progress in Astronautics and Aeronautics; 1994

[6] Özkan B, Özgören MK, Mahmutyazıcıoğlu G. Comparison of the acceleration- and angle-based guidance laws for a short-range air-to-air missile (in Turkish). In: TOK2008-Automatic Control National Meeting. İstanbul, Turkey: İstanbul Technical University; 2008

[7] Kunwar F, Benhabib B. Advanced predictive guidance navigation for mobile robots: A novel strategy for rendezvous in dynamic settings. International Journal on Smart Sensing and Intelligent Systems. 2008;**1**(4):858-890

[8] Özkan B. Investigation of the usefulness of the linear homing guidance law for the motion planning of mechatronic systems. In: 17th International Carpathian Control Conference (ICCC 2016), Tatranská Lomnica, Slovakia; 2016

[9] Tsay TS. Guidance and control laws for quadrotor UAV. WSEAS Transactions on Systems and Control. 2014;**9**(1):606-613

[10] Ogata K. Modern Control Engineering. 2nd ed. New Jersey, USA: Prentice-Hall International Editions; 1990

[11] Voos H, Nourghassemi B. Nonlinear control of stabilized flight and landing for quadrotor UAVs. In: Proceedings of the 24th Annual Meeting of the European Institute for Applied Research (IAR'2009). Góra, Poland: Zielona; 2009

[12] Zhang D, Qi H, Wu X, Xie Y, Xu J. The quadrotor dynamic modeling and indoor target tracking control method. Mathematical Problems in Engineering. 2014;**2014**:1-9

[13] Özkan B. Dynamic modeling, guidance, and control of homing missiles [PhD dissertation]. Ankara, Turkey: Middle East Technical University; 2005